REPORT DOCUMENTATION PAGE

Form Approved OMB No. 0704-0188

1. REPORT DATE *(DD-MM-YYYY)*	2. REPORT TYPE	3. DATES COVERED *(From – To)*
27-05-2010	Final Report	1 November 2007 - 01-Nov-08

4. TITLE AND SUBTITLE

Transport at the nanoscale: integration of micro-macro scales for electro-thermal device simulations

5a. CONTRACT NUMBER
FA8655-08-1-3017

5b. GRANT NUMBER

5c. PROGRAM ELEMENT NUMBER

6. AUTHOR(S)

Dr. Alessandro Pecchia

5d. PROJECT NUMBER

5d. TASK NUMBER

5e. WORK UNIT NUMBER

7. PERFORMING ORGANIZATION NAME(S) AND ADDRESS(ES)

University of Rome 'Tor Vergata'
University of Rome Tor Vergata
Rome 133
Italy

8. PERFORMING ORGANIZATION REPORT NUMBER

N/A

9. SPONSORING/MONITORING AGENCY NAME(S) AND ADDRESS(ES)

EOARD
Unit 4515 BOX 14
APO AE 09421

10. SPONSOR/MONITOR'S ACRONYM(S)

11. SPONSOR/MONITOR'S REPORT NUMBER(S)
Grant 08-3017

12. DISTRIBUTION/AVAILABILITY STATEMENT

Approved for public release; distribution is unlimited.

13. SUPPLEMENTARY NOTES

14. ABSTRACT

In this project we have developed some of the necessary tools and software infrastructure to enable multiscale approaches for electronic transport and heat dissipation in materials and devices. The multiscale-multiphysics concept requires exchange of information between the microscopic and the macroscopic levels of descriptions, allowing simulations of the physical behavior of a material including nanoscale details. This computational paradigm allows to bridge over several orders of magnitudes of scale-lengths and time scales, transferring information between the micro and the macro world or vice-versa. The multiscale and multi physics approach can be applied to the most diverse physical problems and disciplines from biochemistry to materials science. Examples of current working applications range from the chemical behavior of molecular reactions to protein and enzyme functions or ion pumps, the analysis of structural defects and crack formations to problems of surface adhesion and cathalisis. Successful applications have also been reported in the study of photoexcitations, exciton dissociations and charge transfer. In most cases the multiscale approach consists in combining quantum mechanical calculations (QM) with faster semi-empirical or empirical interatomic forces (molecular mechanics). In the last decade several attempts have been made to couple interatomic forces, obtained with semiempirical or empirical potentials, with macroscale simulations, usually performed using nite-elements schemes, describing the materials with average local parameters such as elastic properties, electron/ion mobilities, energy bands, etc. This is the last chain of a whole hierarchy of methods, but hardly easy to accomplish. Coupling macroscopic with atomistic models poses several diculties due to quite heterogeneous frameworks and formalisms involved, since the two approaches have been historically developed by different communities to target substantially different problems.

15. SUBJECT TERMS

EOARD, electro-thermal simulations, nanoscale systems

16. SECURITY CLASSIFICATION OF:			17. LIMITATION OF ABSTRACT	18, NUMBER OF PAGES	19a. NAME OF RESPONSIBLE PERSON
a. REPORT	b. ABSTRACT	c. THIS PAGE			WYNN SANDERS, Maj, USAF
UNCLAS	UNCLAS	UNCLAS	UL	21	19b. TELEPHONE NUMBER *(Include area code)* +44 (0)1895 616 007

Final Research Report

Air Force Grant FA8655-08-1-3017

Transport at the nanoscale: integration of micro-macro scales for electro-thermal device simulations.

Alessandro Pecchia
Dipartimento di Ingegneria Elettronica, Universita degli Studi di Roma "Tor Vergata", via del Politecnico 1, I-00133 Roma, Italy.

Contents

List of Figures

1 Introduction

In this project we have developed some of the necessary tools and software infrastructure to enable multiscale approaches for electronic transport and heat dissipation in materials and devices. The multiscale-multiphysics concept requires exchange of information between the microscopic and the macroscopic levels of descriptions, allowing simulations of the physical behavior of a material including nanoscale details. This computational paradigm allows to bridge over several orders of magnitudes of scale-lengths and time-scales, transferring information between the micro and the macro world or vice-versa. The multiscale and multi physics approach can be applied to the most diverse physical problems and disciplines from biochemistry to materials science. Examples of current working applications range from the chemical behavior of molecular reactions to protein and enzyme functions or ion pumps, the analysis of structural defects and crack formations to problems of surface adhesion and cathalisis. Successful applications have

also been reported in the study of photoexcitations, exciton dissociations and charge transfer. In most cases the multiscale approach consists in combining quantum mechanical calculations (QM) with faster semi-empirical or empirical interatomic forces (molecular mechanics). In the last decade several attempts have been made to couple interatomic forces, obtained with semiempirical or empirical potentials, with macroscale simulations, usually performed using finite-elements schemes, describing the materials with average local parameters such as elastic properties, electron/ion mobilities, energy bands, etc. This is the last chain of a whole hierarchy of methods, but hardly easy to accomplish. Coupling macroscopic with atomistic models poses several difficulties due to quite heterogeneous frameworks and formalisms involved, since the two approaches have been historically developed by different communities to target substantially different problems.

Multiscale approaches can be applied both to obtain macroscopic parameters from microscopic models (*overlap* method) or different scales can be sewed together at some boundary (*bridge* method) in order to treat critical subregions with appropriate models. Both shemes are valid alternatives, depending on the problem to be solved, but bridge methods require micro and macro scales to tightly couple and exchange information in both directions posing additional interfacing challenges. Practical examples of this methodology are the multiscale models developed to compute strain relaxation around a crystal defect or to nanoelectromechanical cantilevers.

The processes of interest in this project are electron and heat transport in materials and devices, where the multiscale concept has not been fully developed yet. Recent technological advances have progressively scaled the active region of electronic and optical devices down to scales of few tents of nanometer or lower. However the nano-world is always addressed via macroscopic contacts that carry the current information. Heat sinks are also of macroscopic size and heat managment has becoming a pressing problem in modern nanoelectronics. It is therefore of crucial importance for the development of the field to couple micro and macro scales in order to address electro-thermal properties. Possible applications of this multiscale coupling range from electrical simulations of nanodevices and their thermal managment. The model will also be applicable, with suitable adaptations, to study heat dissipation in materials where heat is locally produced with mechanisms other than joule heating, for instance as a consequence of light absorption.

The whole point of this research is to build a suitable environement in which electronic and heat transport simulations (performed at FEM level) can be coupled with microscopic models for heat generation and transport. The heat generation rate at the micro scale can be accounted by imposing corresponding boundary conditions at the micro-macro boundaries.

Among the several available software implementing FE calculations, we have chosen the LibMesh library, which is a well established and lively open-source (LGPL) project. Both aspects are quite important when developing

new derivative works, since the feedback from library authors for clarifications and bug fixes may be necessary in many cases. LibMesh contains interfaces to the PETSc and SLEPc numerical solvers and the METIS partitioning library, giving a complete environment for development of general solutions of partial-differential equations based on the FEM approach.

2 Heat dissipation models

2.1 The Fourier transport equations

Heat balance problems at the macroscopic scale are governed by the Fourier's law, which together with the continuity equation reads as:

$$\nabla \cdot (-\kappa \nabla T) = H_S, \tag{1}$$

where κ is the lattice thermal conductivity tensor, T the temperature and H_s is the total heat source. The heat source may be given by any dissipative processes such as light absorption or Joule's effect. The latter can be associated to dissipation induced by carrier transport and can be described at macroscopic scales in terms of a drift-diffusion model. The heat source can be written explicitly in terms of the electron and hole currents and thermoelectric effect,

$$H_S = -\nabla \cdot \left[(P_n T + \phi_n)\mathbf{J_n} + (P_p T + \phi_p)\mathbf{J_p} \right], \tag{2}$$

where ϕ_n and ϕ_p are the electro-chemical potentials and P_n and P_p are the thermoelectric power for electrons and holes given by

$$P_n = -\frac{k_b}{q}\left(\frac{5}{2} + \frac{e\phi_n + E_c - e\varphi}{k_b T}\right) \tag{3}$$

and

$$P_p = \frac{k_b}{q}\left(\frac{5}{2} - \frac{e\phi_p + E_v - e\varphi}{k_b T}\right) \tag{4}$$

The expression 2 can be split, as shown in Table 1

Expression	*Heat source*
$\frac{\lvert\mathbf{J_n}\rvert^2}{\sigma_n}$	*Electrons Joule's effect*
$\frac{\lvert\mathbf{J_p}\rvert^2}{\sigma_p}$	*Holes Joule's effect*
$qR_{SRH}\left(\phi_p - \phi_n + T\left(P_p - P_n\right)\right)$	*Recombination effect*
$-T\mathbf{J_n} \cdot \nabla P_n$	*Electrons Peltier-Thomson effect*
$-T\mathbf{J_p} \cdot \nabla P_p$	*Holes Peltier-Thomson effect*

Table 1: Drift diffusion heat sources

The equations above have been implemented on a finite-element (FEM) solver based on the LIBMESH library. This solver is part of the TiberCAD

simulator under development in the 'Tor Vergata' group. The project can be visioned at the url http://www.tibercad.org.

As a working example we report a 2-dimensional simulation of a PN diode surrounded by air. The finite element meshing of the device is shown in Fig. 1. The temperature at the air boundary was fixed to 300 K and

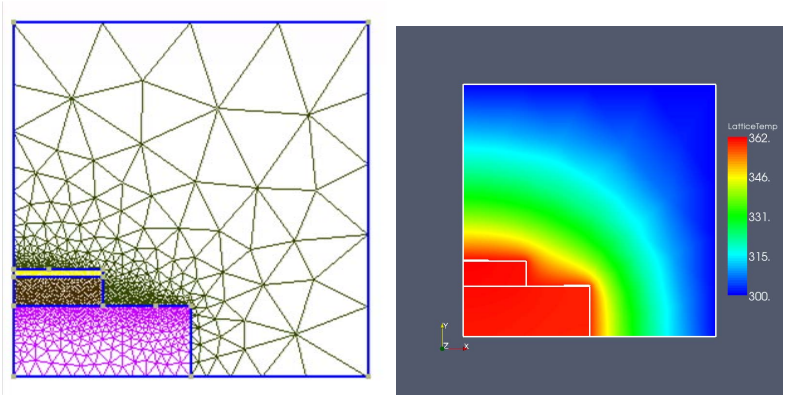

Figure 1: *(Left) Mesh structure and (Right) temperature map of a pn diode*

we have included a thermal surface resistance representing heat dissipation into the substrate. The temperature map reported in Figure 1 refers to a direct bias of the diode and shows a rise of temperature near the pn junction where e/h recombination takes place.

Different types of boundary conditions can be handled already within our tool, namely

- 1. Insulating surface: $\mathbf{J_q} \cdot \mathbf{N} = 0$
- 2. Ideal conducting surface: $T = T_{ext}$
- 3. Thermal resistive surface: $\mathbf{J_q} \cdot \mathbf{N} = G_s(T - T_{ext})$

In the above, J_q is the thermal flux and G_s is the surface thermal conductivity.

As an example of heat generators we have modeled a simple array of dots acting as heat sources. The Fourier transport model is solved by imposing a fixed temperature at the boundary and a realistic source of heat emanating from each dot. The results are shown in figure 2.

2.2 Microscopic theory of heat transport: grey model

As the characteristics length becomes comparable with the phonon mean free path the approximation of local thermal equilibrium introduces a not negligible error. Several models based on the Boltzmann Transport Equation (BTE) have already been proposed in the last decade [1]. We have

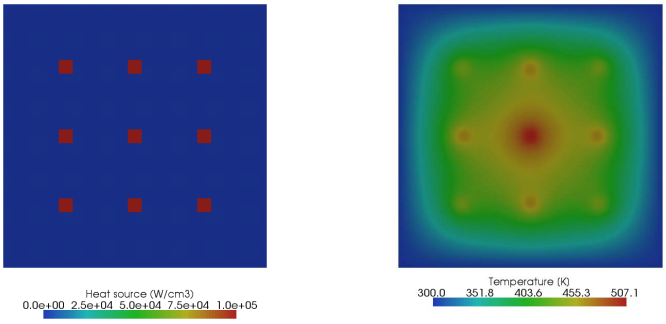

Figure 2: *(Left) Array of heat sources (Right) Temperature map*

explored applications of the so-called grey model [2], which relies on the following assumptions: (i) collision experienced by phonons are described via a relaxation time, which does not depend on the phonon energy; (ii) All phonons are considered to have the same group velocity, equal to the first sound velocity. Neglecting the full phonon dispersion is a severe assumption that will be dropped in future developments. With these assumptions the BTE for phonons is

$$v_g \nabla \cdot \mathbf{s}\varepsilon = \frac{\varepsilon - \varepsilon_0}{\tau} + H \tag{5}$$

where e is the density of phonon energy propagating along the $\mathbf{s}$ direction, v_g is the sound velocity, e_0 the equilibrium energy density, τ the scattering relaxation time and H the total heat source per solid angle. Energy conservation is achieved by setting a global condition on the energy flux over the whole solid angle. As equation (5) needs to be solved for each direction, $\mathbf{s}$, we need to discretize the solid angle. The thermal flux in direction i can be computed using

$$J_q^i = \frac{1}{4\pi} \int_\Omega v_g \varepsilon s_i d\Omega. \tag{6}$$

Finally we relate the local lattice temperature with the density of heat energy using [3]

$$T = T_0 + (\varepsilon - \varepsilon_0) \frac{4\pi}{C(T_0)} \tag{7}$$

where $C(T_0)$ is the heat capacity at the temperature T_0. The all algorithm can be summarized as follows

- 1. Set the first guess as the equilibrium energy density, e_0 and isotropically spread it in all directions.

- 2. Solve Eq. (5) for each direction.

- 3. Compute the new equilibrium energy.

- 4. Go to step 2 until convergence is reached.

Dirichlet boundary conditions can be employed by fixing the generated phonon energy to the desired value. Thermal insulating boundary condition can be applied by considering both specular and diffusive interfaces. The error is calculated for the equilibrium density. It is possible to show that whenever the mean free path becomes much smaller than the device size, the gray model approaches the diffusive limit and Fourier thermal transport is recovered.

2.3 Towards the coupling of micro-macro scales

In this section we show a practical coupling of heat transport models at the micro (grey model) and macro (Fourier) scales. To this end we need to define a general embracing strategy between microscopic and macroscopic domains and define their exchange of information. We need to distinguish between two cases of multiscale couplings. The first situation is when the micro and macro regions spatially coincide. We may call this a *overlapping* condition. This situation could be useful to investigate the properties of molecules embedded in hosting materials, such as polymers or nanostructured media, and may be applied especially to study materials coupled to light-sources, like OLEDs, lasers or energy conversion devices such as organic solar cells. In this case the microscopic calculations will couple to the classical electro-thermal equations in the form of source terms that will reflect the exciton generation recombination and dissociation rates and will also provide power released per unit volume under the form of heat. In the second case, that we may call *bridging*, the microscopic region is embedded within the classical (macroscopic) regions and the two are spatially separated. In this case the two regions communicate via appropriate continuity conditions of the heat flux across the boundary between the two regions. The latter will come from the calculation of the rate of energy flowing at the interface. The models in the two regions will then be solved self-consistently by implementing an appropriate feedback loop. To many respects this situation is more difficult to handle than the first, since the convergence of the macroscopic FEM equations and application of flux boundaries is more delicate. For this reason the bridge case has been here analyzed in detail in order to asses the feasibility of the approach.

In principle, we might perform the BTE over the whole domain, but the discretization over the solid angle would strongly increase the computational effort. For this reason we compute the BTE only in the region where it is needed (micro domain) and the Fourier model is applied to the rest of the device (macro domain). Both models can communicate through their boundary conditions in a bridge scheme. The Fourier domain fixes the boundary temperature to the grey model. Conversely, the latter fixes the heat flux to the Fourier model. The self-consistent scheme that we have developed can be summarized as follows

- 1. Solve the Fourier model on the whole domain (micro and macro) which fixes the boundary temperature on the micro domain.

- 2. Solve the gray model on the micro domain which imposes the boundary heat flux on the macro domain.

- 3. Solve the Fourier model on the macro domain.

- 4. Go to step 2 if the convergence is not reached.

In order to speed-up convergence we find that a crucial ingredient is the first guess of the equilibrium energy density. A good guess was obtained by computing the Fourier heat transport over the whole device, including the microscopic region. On the other hand we find that whenever the grey domain becomes larger than the phonon mean free path, the number of steps required for convergence significantly increases.

2.4 Application to a GaN-QD embedded in AlGaN

The method is applied on a system comprising a 5 nm GaN cubic quantum dot embedded in a nanocolumn of $Al_{0.2}GaN$ of 100 nm in height. The two contacts are p and n doped 1^{19} cm^{-3}, respectively. The QD is surrounded by a buffer layer of intrinsic $Al_{0.2}GaN$ (see Fig. 1). We first compute the I-V characteristics of the device within the drift diffusion model, showing a diode behaviour, as expected. Joule heat is generated by holes and electron transport, as shown in Figure 3 The dominant contribution of heat due to recombination within the QD. The solid angle for the integration of the grey model equation is discretized in 18 parts (6 the azimut angle and 3 the elevation angle). Sounds velocity and thermal conductivities of GaN and AlN are taken from the literature [4]. Thermal relaxation times are computed from the relation $3\kappa/(Cv_g^2)$ in order to be consistent with the diffusive limit

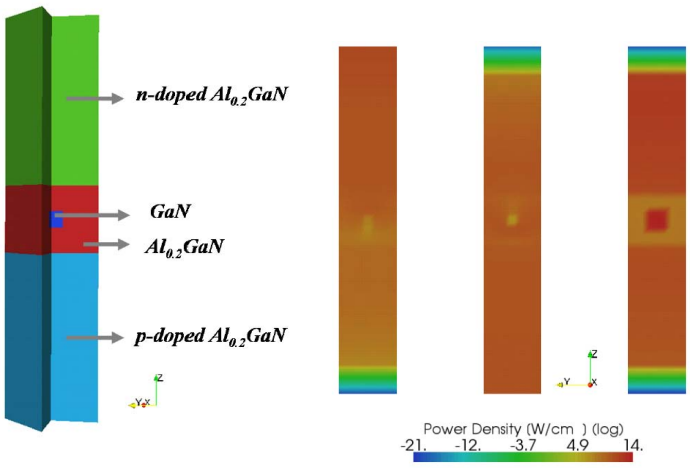

Figure 3: *(Left) Structure of a Nanocolum with a QD. (Right) heat sources due to n and p joule effects and recombination heat*

[3]. The sound velocity of the AlGaN is obtained by relying on the virtual crystal approximation as in [4]. As boundary conditions at end of the two contacts we set the temperature of 300 K. As shown in Fig. 4 the BTE and the Fourier model give a maximum temperature of about 334 K and 319 K, respectively, revealing that that phonons distribution is far away from the local equilibrium. Furthermore, the BTE model gives a strongly peaked temperature across the quantum dot region, resulting in a more realistic temperature profile. Lets now consider the multiscale approach. The grey

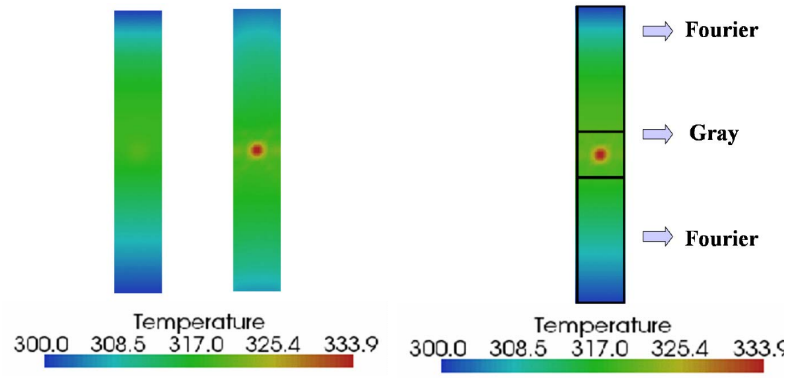

Figure 4: *(Left panel) Comparison of temperature profiles from Fourier and gray model. (Right panel) Multiscale coupling of Fourier and grey models.*

model is applied to the micro domain which includes the quantum dot and

the buffer regions, whereas the contacts belong to the macro domain, treated with the Fourier model. The two models are solved self-consistently as outlined above. The temperature profile, as shown in the right panel of Fig. 4, matches the BTE model performed over the whole domain. In fact one may expect at first that the multiscale temperature profile should matches the Fourier solution in the regions where Fourier is solved. However, we should bare in mind that the multiscale solution *knows* about the BTE solved in the QD region, which leads to a different effective boundary condition for the temperature at the micro/macro interface, reflected in a different temperature profile. On the other hand, the Fourier model and the gray model correctly approach each other at length-scales larger than the phonon mean free path. We finally point out that the size of the micro region is a crucial choice that depends on the phonon mean free path and the lattice thermal conductivity, as well as the magnitude of the heat source. Since the temperature affects the energy gap, the optical recombination spectrum can be influenced by the heat transport model. As shown in Fig. 5 the energy peak undergoes a red shift of about 10 meV when the BTE is employed in place of the Fourier model.

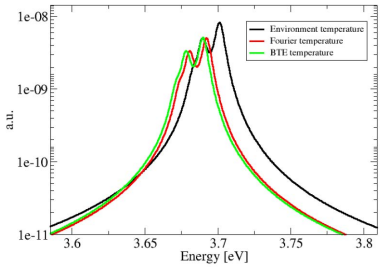

Figure 5: *Optical recombination spectrum in the QD obtained for different thermal models.*

2.5 Conclusions

A multiscale scheme for thermal modeling of nanostructures has been developed and applied to a GaN quantum dot embedded in a AlGaN nanocolumn. Temperature results of Fourier, BTE and multiscale models are compared. We found out that the Fourier model underestimates the temperature across the quantum dot and justifies the need of a BTE based model. The maximum temperature, across the dot, is about 319 K for the Fourier model, against 334 K of the BTE model. We further identified a convenient choice of the initial guess of equilibrium energy density, which strongly speeds up the loop convergence of the gray model. Finally, we investigated the influence of the used model on the optical spectrum.

3 Heat dissipation in molecular junctions

The first step of development consists in formulating a microscopic theory of heat dissipation due to joule heating in nanojunctions. We focus our attention to molecular bridges as for instance those obtained in nanopores, break-junctions or STM configurations. This description can be later extended to other types of electronic nanojunctions, such as semiconducting quantum dots or quantum wells.

At the microscopic level, the release of energy in a molecular junction is described by a quantum mechanical approach, fully including the electron-phonon coupling. Molecular vibrations and electron-vibron couplings are treated in the usual way [5, 6, 7, 8], after decoupling the Hamiltonian as a superposition of independent one-dimensional oscillators corresponding to the normal modes of vibrations, labeled by q. The harmonic oscillators can be quantized following the usual prescriptions, by making use of the standard relationships between the position operator and the creation/annihilation field operators, a_q^+ and a_q. Therefore, the ionic vibrations of a molecular wire can be described as a class of bosonic particles, here referred as *phonons*. The result is a term in the Hamiltonian describing the electron-phonon coupling,

$$H_{el-ph} = \sum_{q,\mu,\nu} \gamma_{\mu\nu}^q c_\mu^+ c_\nu \left[a_q^+ + a_q \right], \tag{8}$$

where c_μ^+ and c_ν are, respectively, the creation and annihilation operators of one electron in the atomic basis-set and $\gamma_{\mu\nu}^q$ are the electron-phonon coupling matrices. M_q are the atomic masses, ω_q the mode frequencies and $\mathbf{e}_\alpha^q$ are the normalized atomic displacements for each mode. The non-orthogonality of the atomic basis-set is reflected by the presence of the overlap matrix, $\mathrm{S}_{\mu\nu}$, and its derivative with respect to the ionic positions, R_α.

While crossing the system, electrons interact with the molecular ionic vibrations from which they can be inelastically scattered. The formalism of our choice is the non-equilibrium Green's function approach, which is very well suited to study such problems. The electron-phonon interaction is treated within perturbation theory of the non-equilibrium Green's function formalism and the current through the junction is computed using the Meir-Wingreen formula [9] which contains an elastic and an inelastic term. The electron-phonon self-energy can be evaluated with diagrammatic techniques such as the self-consistent Born approximation (SCBA).

$$\Sigma_{ph}^{<(>)}(\omega) = i \sum_q \int_{-\infty}^{+\infty} \frac{d\omega'}{2\pi} \gamma_q G^{<(>)}(\omega - \omega') \gamma_q D_q^{<(>)}(\omega'), \tag{9}$$

where $D_q^{<(>)}$ are the correlation functions related to the vibrational modes. Explicit forms for the self-energy can be found when the vibrations are assumed Einstein oscillators with delta-like density of states. Such forms are presented in [10, 11].

3.1 Phonon rate equation

When a bias is applied and a current starts to flow, the interaction between electrons and vibrations drives the population of phonons out of equilibrium. That is, the distribution of phonons deviates from a simple Bose-Einstein distribution due to phonon emission and absorption processes. Moreover, the presence of the leads allows the relaxation of phonons from the device into the contacts. In order to describe these processes, a semi-classical rate equation has been implemented [10],

$$\frac{dN_q}{dt} = R_q - J_q[N_q - n_q(T_0)], \tag{10}$$

where N_q is the non-equilibrium phonon population, $n_q(T_0)$ is the equilibrium phonon distribution at temperature T_0, and R_q is the net rate of phonons emitted. This rate is computed from the emitted power in each mode, P_q, which can be computed according to the NEGF theory [10],

$$P_q = \frac{2}{h}\int_{-\infty}^{+\infty} \mathsf{Tr}\left[\Sigma_{ph}^{<}(E)G^{>}(E) - \Sigma_{ph}^{>}(E)G^{<}(E)\right] EdE. \tag{11}$$

The emission rate in each mode, R_q, can be defined as $R_q = P_q/\hbar\omega_q$, which can be also expressed in terms of absorption and emission processes [10], A_q and E_q,

$$R_q = [(N_q + 1)E_q - N_q A_q]. \tag{12}$$

The calculation details of these functions can be found in [10] and [11]. Under stationary conditions, equations (10) and (12) can be combined to give the explicit solution

$$N_q = \frac{n_q(T_0)J_q + E_q}{J_q + A_q - E_q}. \tag{13}$$

This is a central result of our model. As an important consistence check, we could show that under equilibrium condition (no applied bias), $A_q = 0$ and $E_q = 0$ and consequently, $N_q = n_q(T_0)$.

3.2 Phonon-phonon decay rates into the contacts

The power dissipation from the molecule to the contacts is described by the rates J_q. These can be computed from first principles or treated as parameters. The calculation is performed by setting up the full Hessian and partitioning it in the same way as the Hamiltonian, namely into device region and contacts. A Green's function is then built for the vibrational eigensystem:

$$\sum_j \mathcal{H}_{ij} e_j^q = \sum_j \mathcal{M}_{ij} e_j^q \omega_q^2, \tag{14}$$

using open boundary conditions, as usual. In the previous equation $\mathcal{H}_{ij}$ is a matrix element of the Hessian, e_j^q are the normal modes of vibration, $\mathcal{M}_{ij}$ is the mass matrix element and ω_q is the frequency of the mode. From (14) it is possible to construct a self-energy for the phonons, whose imaginary part can be used to extract the phonon relaxation lifetime [11].

This is essentially a Fermi Golden Rule treatment including first order one phonon to one phonon decay processes. It neglects a large number of other decay channels, for example related to anharmonic effects. Particularly, high frequency modes do not couple directly with the phonon band of the contacts, meaning that only one phonon to many phonons decay processes are relevant in describing such relaxation mechanisms. Some of these effects can be partially included by defining an effective phonon density of the contact modes. The formal Green's function for the phonons is

$$G_p^r(\omega^2) = \frac{1}{\mathcal{M}_i\omega^2 - \mathcal{H}_M - \Pi_L^r(\omega^2) - \Pi_R^r(\omega^2)} \tag{15}$$

where the self-energies $\Pi_{L,R}^r(\omega^2)$ map the infinite contacts into the finite portion of the device. The real part of the self-energies represent a shift of the frequencies of the normal modes of the extended molecule induced by the coupling of that region with the bath, the imaginary part instead describes the phonon-phonon decaying process, J_q.

3.3 Definition of molecular temperature

For the purpose of our studies we define an effective molecular temperature, T_m, as a direct measure of the internal energy stored in the vibrational degrees of freedom. T_m is found by imposing the following identity,

$$U = \sum_q \hbar\omega_q N_q = \sum_q \frac{\hbar\omega_q}{exp(\frac{\hbar\omega}{k_b T_m}) - 1}, \tag{16}$$

where U is the total internal energy.

As shown in the following section, as well as in several reports [10, 11, 12], this temperature parameter faithfully maps the internal energy and can be considered as an equivalent measure of this quantity. We could also think in terms of a nanoprobe put in contact with the molecule and able to locally measure its temperature. Although this system has not been experimentally realized yet, we can think at it as a *gedanken experiment*. A thermometer registers a temperature as a consequence of an equilibration process. Such an equilibration is a consequence of an energy exchange between molecule and thermometer. The energy flux between the two systems stops at equilibrium, that can be expressed by

$$\sum_q \hbar J_q \omega_q N_q = \sum_q J_q \frac{\hbar\omega_q}{n}_0(T_p), \tag{17}$$

where J_q is the rate of phonon decays from the molecule to the bath and $n_0(T_p)$ is the equilibrium distribution of phonons in the thermometer, with temperature T_p. Assuming the decay rates all equal, we arrive to the conclusion that $T_p = T_m$.

3.4 Applications to fullerene on Cu and Si

The model described above has been applied to several systems. The basic focus of our investigations has been joule heating and cracking of fullerene molecules in STM configurations.

We have considered two prototype systems: C_{60} on Cu(110) and C_{60} on Si(100). These represent a molecule on a metallic and a semiconducting surfaces, and can be useful to understand different behaviors due to metallic bands and bandgaps. The method of choice for our calculation is the density-functional tight-binding method (DFTB). The geometries of the two structures, fully relaxed at the DFTB level, are shown in figure (6). Good agreement is found with respect to previous literature.

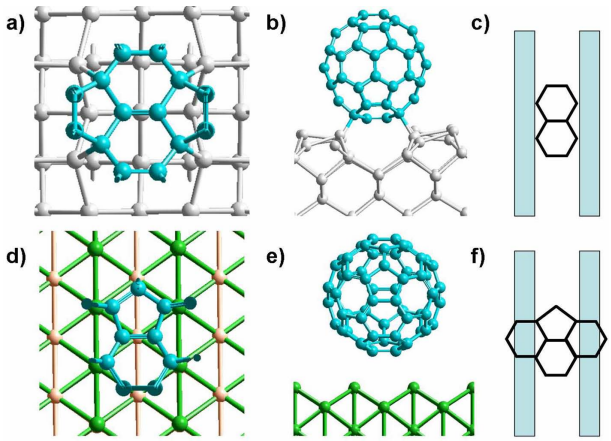

Figure 6: Geometries of C_{60} relaxed on two different surfaces. **i)** Si(100): a) top view on the lowest fullerene atoms close to the silicon surface, b) side view, c) sketch of the bonding site. **ii)** Cu(110): d), e), f) the same as for silicon.

The coupling between the phonons of the substrate and the vibrations of the molecule can be quantified by the local density of states (LDOS), is shown in figure (7).

This calculations are performed according to section 3.2, using the dynamical matrix (Hessian) as produced by the DFTB code.

In the background the surface density of states for the phonons of the isolated substrates is shown. The silicon substrate (figure 7(a)) has a Debye frequency of 650 cm^{-1}, while for the much heavier copper atoms it is only 400 cm^{-1} (figure 7(b)). The broadenings of the molecular vibrations are

directly proportional to the decay rates into the contact reservoirs, the J_q coefficient of (10). It is easy to observe, that the broadening becomes very narrow beyond the Debye frequency. Moreover, as expected, the broadening induced by the silicon substrate for the modes below the Debye frequency is substantially larger (corresponding to a rate of 10^{12} Hz) than the broadening for the copper substrate (10^{11} Hz). This is a straightforward consequence of the higher mass of copper compared to silicon. In order to compute the

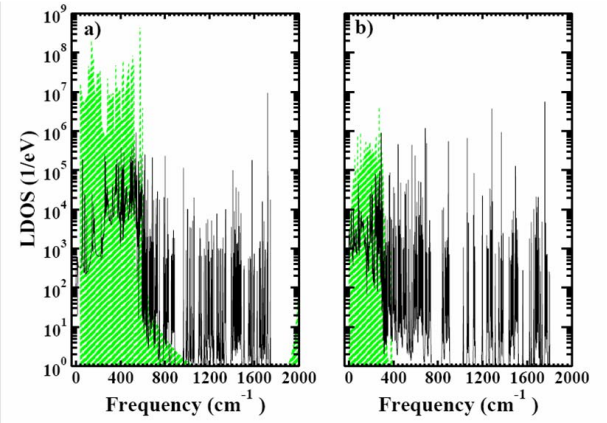

Figure 7: The phonon LDOS for the two systems, **a)** C_{60} on Si(100) and **b)** C_{60} on Cu(110). The black line represents the LDOS with broadening induced by coupling to the surface modes. In the background, the shaded areas represent the phonon density of states for the isolated substrates.

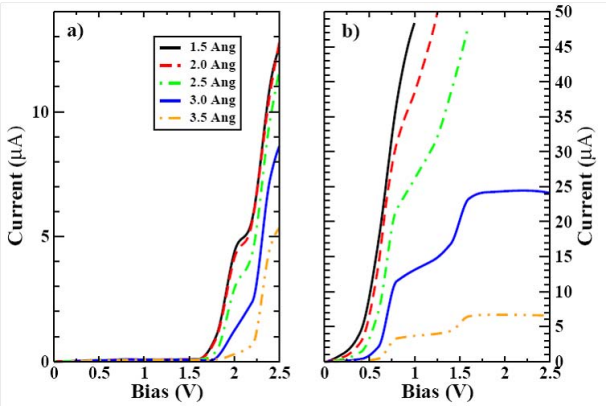

Figure 8: Calculated I-V characteristics. **a)** C_{60} on Si(100), **b)** C_{60} on Cu(110).

current through the system a second contact has been added to the geometry. A copper STM tip was used in both cases, In all our simulations the substrate and tip where assumed to be at T=0 K. The I-V characteristics are plotted

in figure (8) for different tip-molecule distances. The silicon substrate was assumed heavily p-doped in order to make it conducting, with a Fermi energy at the valence band edge with a carrier concentration of 10^{19} holes cm^{-3}. For both systems under investigation the tip-molecule distance (Z) and the bias (V) control the molecular temperature, however, in the case of the silicon substrate the energy gap also plays an important role. The temperature of C_{60} on silicon is shown in figure (9) together with the electronic LDOS of the molecule. Due to the energy gap the molecular states of C_{60} couple only weakly to the substrate, giving rise to a sharp, delta-like shape of the states in the LDOS. This small broadening is reflected in the low conductivity within the gap region.

Steps in molecular temperature are observed when molecular resonances enter the conduction window. However, due to energy conservation, the electron-phonon emission from (**??**) is related to the Green's function evaluated at an energy shifted by ω_q. Hence the resonance is fully effective only at a bias beyond $V_{res} + \omega_{max}$, where V_{res} is the bias at which the resonance enters in conduction and ω_{max} is the largest frequency of the molecule. In our fullerene case, this leads to a shift of 0.2 V between V_{res} and the energy position of the temperature step.

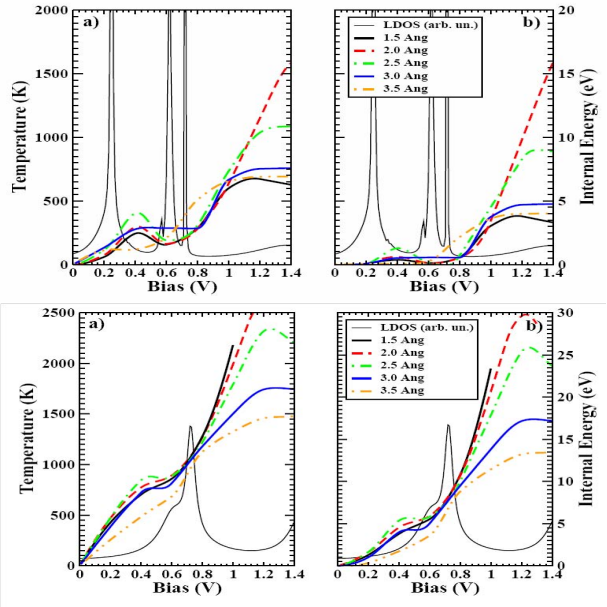

Figure 9: C_{60} on Si(100) (Top) and Cu(110) (Bottom). **a)** temperature in the junction for different tip-molecule distances, **b)** internal energy, U_m, for different tip-molecule distances.

A similar behavior can be noticed for the fullerene on copper shown in figure (9). Comparing the temperature curves of figure (9) and figure (9),

some important differences can be noticed. The temperature for the copper substrate increases much faster than the Si counterpart.

One may expect that the reason for this is simply the higher current observed for the Cu substrate, leading to a larger joule heating. However, if we carefully inspect the two curves we find that this conclusion is deceptive. At 1 V the C_{60} temperature on Si is 700 K against 1950 K on copper for a tip-molecule distance of 2 Å. However, the current is 0.1 μA on silicon compared to 40 μA on copper, therefore 400 times smaller. Based on the current argument we should expect a much lower temperature for the Si substrate (or a much larger temperature on Cu).

The reason for this discrepancy can be traced back to electron-hole (EH) pair excitations, playing the role of an important damping mechanism. In metal this effect is quite relevant and cools the molecule down.

On the other hand, on the silicon substrate the EH mechanism is inactive because of the energy gap and the heating, despite a stronger bonding and a larger phonon coupling, is faster. Further important evidence for the relevance of the electron-hole cooling mechanism can be seen in the temperature curve obtained for silicon by playing with the molecule-tip distance as shown in figure (9). Increasing the tip-molecule distance has two opposite effects. On the one hand it decreases the molecular temperature due to current lowering, on the other hand it also decreases the EH damping mechanism, favoring heating. This explains why on Si, the molecular temperature tends to increase when the tip moves from 1.5 Å to 2.0 Å. In this case the second mechanism prevails over the first.

The model and the calculations presented above have been also applied to the understanding of the cracking experiment of fullerenes on Cu by the approaching of an STM tip with a fixed voltage [13]. In order to understand the observed I-V characteristics before the C_{60} irreversibly deteriorates we have fitted the experimental data with our model by defining a critical temperature above which we assume the fullerene has cracked. This temperature is found at about 1600 K. From the critical temperature we can extract a critical tip distance and a critical current/voltage. Figure 10 shows the important achievements of our theory. The critical current (I_{dec} is plotted vs the critical voltage V_{dec} and agrees well with the experimental behavior as discussed in [13]. An important point is that that our model support the explanation that the molecule can support high currents when the tip is in contact because electron/hole excitations provide a good absorption channel keeping the molecule cool.

3.5 Conclusions

In conclusion of this section, we are satisfied with the microscopic theory of heat dissipation that we have implemented. The fundamental parameters which have been defined in the model are the rate of phonons emitted,

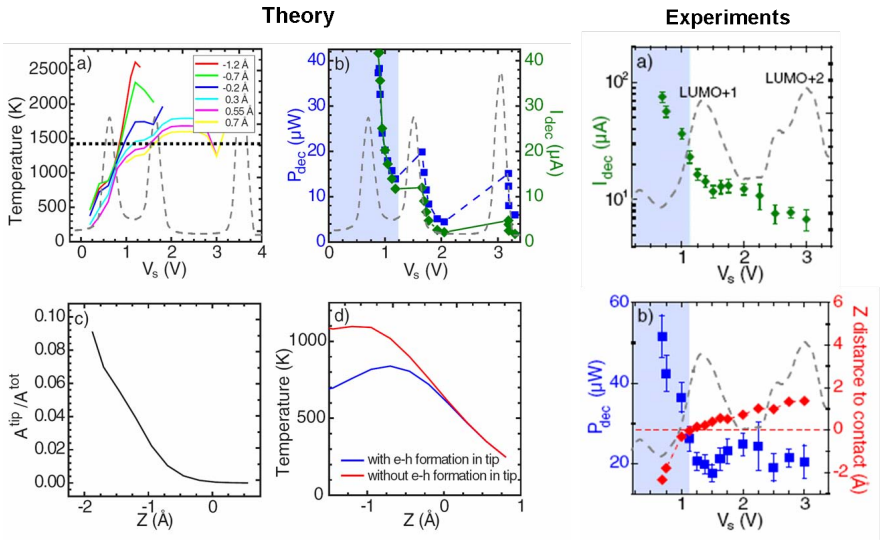

Figure 10: Right. (a) Molecular temperature due to the flow of electronic current as a function of bias for the indicated distances. (b) The values I_{dec} (triangle, green continuous line) and P_{dec} (circle, blue broken line) are marked for a threshold temperature of 1650 K of the C60 molecule. The black dashed line plots the position of the resonances. The blue shaded area marks the contact regime. (c) Ratio of electron-hole pairs in the tip to total number of electron-hole pairs in the junction as a function of tip-molecule distance (at 0.4 V). (d) Temperature T_m at 0.4 V as a function of tip-sample distance with (blue) and without (red) electron-hole pair formation in the tip. Left. Experimental results.

E_q, and the rate of phonon absorbed, A_q, in each vibrational mode due to electron-phonon coupling and the rate of phonon dissipated into the heat reservoirs, J_q, due to phonon-phonon decay rates. These parameters have been calculated from first-principles in order to account for molecular heating as a consequence of a current flux. Adaptations could be provided to other mechanisms, for which a detailed microscopic model should be provided. For instance it would be possible to include sources of heat generated by non-radiative exciton recombinations or relaxations of Frank-Condon excitations after photon absorption.

4 Averall conclusions and outlooks

In conclusion we have shown different heat transport approaches, valid at different length-scales ranging from macroscopic domains, where the Fourier heat transport model is appropriate, to mesoscale where Boltzmann transport should be applied down to nanoscale (molecular) level where full quantum mechanical approaches are necessary. In the latter case we solve the

quantum dissipation within the non-equilibrium Green's function framework. Different scales can be coupled in a self-consistent manner. The *bridge* multiscale approach must be applied in this context, where different model domains must be coupled via boundary conditions on temperature and energy fluxes. As an example of this we have shown the coupling of the gray transport model and the Fourier model. As a future development of the method we plan to demonstrate the coupling of the quantum dissipation model in molecular bridges with the gray model and the Fourier model. At the interface between quantum region and contact region we will impose the heat sources computed within the nanoscale approach and set a Fourier or gray model transport equation for a self-consistent solution. This approach will enable us to evaluate the non-equilibrium temperature of the nanoscale contacting leads, usually assumed in equilibrium in molecular electronics calculations. This will give us one of the first examples of a multiscale/multiphysics approach to the dissipation problem in nanoscale conductors that can cover length-scales from few nanometers up to micrometers.

5 References

References

[1] V J Sreekant, J Y M Narumanchi, and C H Amon. Boltzmann transport equation-based thermal modeling approaches for hotspots in microelectronic. *Heat and Mass Transfer*, 42:478491, 2006.

[2] R Escobar, S Ghai, M S Jhon, and C H Amon. Multi-length and time scale thermal transport using the lattice boltzmann method with application to electronics cooling. *International Journal of Heat and Mass Transfer*, 49:97, 2006.

[3] D G Cahill, W K Ford, K E Goodson, G D Mahan, A Majumdar, H J Maris, R Merlin, and S R Phillpot. Nanoscale thermal transport. *J. Appl. Phys. (Appl. Phys. Rev.)*, 93:793, 2003.

[4] Y. Varshni. Temperature dependence of the energy gap in semiconductors. *Physica*, 34:1, 1967.

[5] N Mingo and K Makoshi. Calculation of the inelastic scanning tunneling image of acetylene on cu(100). *Phys. Rev. Lett.*, 84:3694, 2000.

[6] E G Emberly and G Kirczenow. Landauer theory, inelastic scattering, and electron transport in molecular wires. *Phys. Rev. B*, 61:5740, 2000.

[7] H Ness and A J Fisher. Coherent electron injection and transport in molecular wires: inelastic tunneling and electron-phonon interactions. *Chem. Phys.*, 281:279, 2002.

[8] B Dong, H L Cui, and X L Lei. Photon-phonon-assisted tunneling through a single molecule quantum dot. *Phys. Rev. B*, 69:205315, 2004.

[9] Y Meir and N S Wingreen. Landauer formula for the current through an interacting electron region. *Phys. Rev. Lett.*, 68:2512, 1992.

[10] A Pecchia, G Romano, and A Di Carlo. Theory of heat dissipation in molecular electronics. *Phys. Rew. B*, 74:63, 2006.

[11] G. Romano, A. Pecchia, and A Di Carlo. Coupling of molecular vibrons with contact phonon reservoirs. *J. Phys. Cond. Matt.*, 19:215207, 2007.

[12] A Pecchia, G. Romano, A. Gagliardi, and A Di Carlo. Joule heating of a c_60 nanojunction. *J. of Comp. Elec.*, 6:xxx, 2008.

[13] G Schulze, K J Franke, A Gagliardi, G Romano, C S Lin, A L Rosa, T A Niehaus, Th Frauenheim, G Romano, A Pecchia, and A Di Carlo. Resonant electron heating and molecular phonon cooling in single c60 junctions. *Phys Rev Lett*, 100:136801, 2008.